

$B \rightarrow \rho l \nu$ form factors in lattice QCD

UKQCD Collaboration

K.C. Bowler, J.F. Gill, C.M. Maynard,

School of Physics, University of Edinburgh, Edinburgh, EH9 3JZ, UK

J.M. Flynn

School of Physics & Astronomy, University of Southampton, Southampton, SO17 1BJ, UK

ABSTRACT: We present results from quenched lattice QCD for the form factors for the decay $B \rightarrow \rho l \nu$. The calculations are performed using a nonperturbatively improved action and operators at two values of the lattice spacing. The bottom quark mass is reached by extrapolation from simulations performed with heavy quark masses around the charm mass. Our primary result is for the partially integrated decay rate Γ_{PI} over the range $12.7 \text{ GeV}^2 < q^2 < 18.2 \text{ GeV}^2$:

$$\Gamma_{\text{PI}} = 4.9^{+12+0}_{-10-14} \times 10^{12} \text{ s}^{-1} |V_{\text{ub}}|^2.$$

KEYWORDS: lat qkm lde bph.

Contents

1. Introduction	1
2. Details of the calculation	3
2.1 Improved action and operators	3
2.2 Simulation details	4
2.3 Correlation functions	5
2.4 Light quark dependence	7
2.5 Heavy quark extrapolation	9
3. Results	9
3.1 Systematic uncertainties	12

1. Introduction

One of the primary goals of modern particle physics experiments is to determine the elements of the Cabibbo-Kobayashi-Maskawa (CKM) matrix. This matrix is unitary in the Standard Model (SM) and so-called unitarity triangles can be constructed using the orthogonality of pairs of rows or columns. For the most common triangle, drawn in the complex ρ - η plane of the Wolfenstein parameterisation of the CKM matrix [1], BaBar and Belle have produced the most accurate measurements of one of the angles (via $\sin 2\beta$) to date [2, 3]. To fully constrain the triangle one needs to know the length of the opposing side, governed by V_{ub} . Any process in which a b quark transforms to a u quark can be used to measure V_{ub} . Two possibilities are the exclusive decays $B \rightarrow \pi l \nu$ and $B \rightarrow \rho l \nu$. The form factors which parameterise the hadronic amplitudes for these decays can be determined from first principles in lattice QCD. Combining these with measurements of the decay rate would allow the determination of V_{ub} . In particular, combining a measured differential decay rate with the lattice values for the form factors at high q^2 would allow V_{ub} to be extracted independently of any model for the q^2 behaviour of the form factors.

The transition amplitude for semileptonic decays factorises into leptonic and hadronic parts when $q^2 \ll m_W^2$, where q^2 is the momentum transfer squared and m_W is the mass of the W boson. The hadronic matrix element contains the non-perturbative strong interaction effects and is the largest source of uncertainty in theoretical determinations of the decay rates.

The hadronic matrix elements for $B \rightarrow \rho l \nu$ are parameterised by four form factors

$$\langle \rho(\vec{k}), \eta | V_\mu | B(\vec{p}) \rangle = \frac{2V(q^2)}{m_B + m_\rho} \varepsilon_{\mu\rho\sigma\delta} p^\rho k^\sigma \eta^{\star\delta} \quad (1.1)$$

$$\begin{aligned} \langle \rho(\vec{k}), \eta | A_\mu | B(\vec{p}) \rangle &= i(m_B + m_\rho) A_1(q^2) g_{\mu\sigma} \eta_r^{\star\sigma} - \frac{iA_2(q^2)}{m_B + m_\rho} (p + k)_\mu q_\sigma \eta_r^{\star\sigma} \\ &\quad + \frac{2im_\rho A(q^2)}{q^2} (p - k)_\mu (p + k)_\sigma \eta_r^{\star\sigma} \end{aligned} \quad (1.2)$$

where B is the initial state pseudoscalar meson with three-momentum \vec{p} , ρ is the final state vector meson with three-momentum \vec{k} and polarisation η , and $q = p - k$. The form factor A can be written as

$$A(q^2) = A_0(q^2) - A_3(q^2) \quad (1.3)$$

where

$$A_3(q^2) = \frac{m_B + m_\rho}{2m_\rho} A_1(q^2) - \frac{m_B - m_\rho}{2m_\rho} A_2(q^2) \quad (1.4)$$

with $A_0(0) = A_3(0)$.

In the limit of zero lepton mass the differential decay rate is given by [4]

$$\frac{d\Gamma}{dq^2} = \frac{G_F^2 |V_{ub}|^2}{192\pi^3 m_B^3} q^2 [\lambda(q^2)]^{\frac{1}{2}} \left(|H^0(q^2)|^2 + |H^+(q^2)|^2 + |H^-(q^2)|^2 \right) \quad (1.5)$$

where

$$H^0(q^2) = \frac{1}{2m_\rho \sqrt{q^2}} \left\{ \frac{4m_B^2 |\vec{k}|^2}{m_B + m_\rho} A_2(q^2) - (m_B^2 - m_\rho^2 - q^2) (m_B + m_\rho) A_1(q^2) \right\}, \quad (1.6)$$

$$H^\pm(q^2) = (m_B + m_\rho) A_1(q^2) \pm \frac{2m_B |\vec{k}|}{m_B + m_\rho} V(q^2). \quad (1.7)$$

G_F is the Fermi constant and λ is the kinematic factor,

$$\lambda(q^2) = (m_B^2 + m_\rho^2 - q^2)^2 - 4m_B^2 m_\rho^2 \quad (1.8)$$

V_{ub} can be extracted from the experimental decay rate once the theoretical rate has been determined. The form factors H_0 and H_\pm correspond to the contributions of longitudinally and transversely polarised light vector mesons respectively [5].

We present results for the form factors of the decays $B \rightarrow \rho l \nu$ determined in the quenched approximation to lattice QCD, at two values of the lattice spacing. We use the non-perturbatively (NP) improved Sheikholeslami-Wohlert (SW) [6] action and improved operators. Lattice artefacts then appear formally at $\mathcal{O}(a^2)$ (where a is the lattice spacing) rather than $\mathcal{O}(a)$, though this does not guarantee that they are numerically small.

Mass-dependent lattice artefacts depending on $(am_Q)^2$ in the NP improved renormalisation scheme limit the heavy quark mass m_Q at which one can simulate, without resorting to an effective action such as the Fermilab formalism [7]. We have simulated heavy quarks with several different masses around the charm quark mass, then used continuum Heavy Quark Symmetry (HQS) to motivate the form of our extrapolation to the b quark mass.

In this way am_Q and thus $(am_Q)^n$ are less than one. We have already presented a determination of the form factors for $B \rightarrow \pi l \nu$ at our finest value of the lattice spacing [8].

The rest of the paper is organised as follows. Section two describes the details of the calculation and how the form factors were extracted from the data and then interpolated and extrapolated to physical quark masses. Section three discusses the results and contains an analysis of systematic errors.

The results reported here represent a new analysis of the data used for an earlier preliminary analysis in [9].

2. Details of the calculation

2.1 Improved action and operators

In the Wilson formulation of lattice QCD, the fermionic part of the action has lattice artefacts of $\mathcal{O}(a)$, while the gauge action differs from the continuum Yang-Mills action by terms of $\mathcal{O}(a^2)$. To leading order in a the Symanzik improvement program involves adding the SW term to the fermionic Wilson action,

$$S_{\text{SW}} = S_{\text{W}} - c_{\text{SW}} \frac{i\kappa}{2} \sum_x \bar{\psi}(x) i\sigma_{\mu\nu} F_{\mu\nu}(x) \psi(x) \quad (2.1)$$

Full $\mathcal{O}(a)$ improvement of on-shell matrix elements also requires that the currents are suitably improved. The improved vector current is

$$\begin{aligned} V_\mu^{\text{I}}(x) &= V_\mu(x) + ac_V \tilde{\partial}_\nu T_{\mu\nu}(x) \\ A_\mu^{\text{I}}(x) &= A_\mu(x) + ac_A \tilde{\partial}_\mu P(x) \end{aligned} \quad (2.2)$$

where

$$\begin{aligned} V_\mu(x) &= \bar{\psi}(x) \gamma_\mu \psi(x) \\ A_\mu(x) &= \bar{\psi}(x) \gamma_\mu \gamma_5 \psi(x) \\ P(x) &= \bar{\psi}(x) \gamma_5 \psi(x) \\ T_{\mu\nu}(x) &= \bar{\psi}(x) i\sigma_{\mu\nu} \psi(x) \end{aligned}$$

and $\tilde{\partial}_\mu$ is the symmetric lattice derivative. The current renormalisation is as follows ($J = A, V$):

$$J^{\text{R}} = Z_J (1 + b_J am_q) J^{\text{I}} \quad (2.3)$$

where Z_J is calculated in a mass-independent renormalisation scheme.

The bare quark mass, am_q , is

$$am_q = \frac{1}{2} \left(\frac{1}{\kappa} - \frac{1}{\kappa_{\text{crit}}} \right) \quad (2.4)$$

where κ is the hopping parameter. For non-degenerate currents, an effective quark mass is used in the definition of the renormalised current, corresponding to

$$\frac{1}{\kappa_{\text{eff}}} = \frac{1}{2} \left(\frac{1}{\kappa_1} + \frac{1}{\kappa_2} \right) \quad (2.5)$$

In this renormalisation scheme, the improved quark mass, used in the chiral extrapolations, is defined as

$$\tilde{m}_q = m_q(1 + b_m a m_q) \quad (2.6)$$

2.2 Simulation details

Gauge field configurations were generated using a combination of the over-relaxed [10, 11] and the Cabibbo-Marinari [12] algorithms with periodic boundary conditions at two values of the gauge coupling $\beta = 6/g_0^2$. At each β , heavy quark propagators were computed at four values of the hopping parameter, corresponding to quarks with masses in the region of the charm quark mass. For light quarks, three values of κ were used for the light quark which occurs in the current, the active quark (A), and, owing to disk space constraints, only two values of κ for the passive quark (P). All the light quarks had masses around that of the strange quark. Table 1 lists the input parameters. κ_{crit} , the value of the hopping

	$\beta = 6.2$	$\beta = 6.0$
Volume	$24^3 \times 48$	$16^3 \times 48$
c_{SW}	1.614	1.769
N_{configs}	216	305
a^{-1} (GeV)	2.91^{+1}_{-1}	2.12^{+1}_{-1}
Heavy κ	0.1200, 0.1233, 0.1266, 0.1299	0.1123, 0.1173, 0.1223, 0.1273
Light κ	0.1346, 0.1351, 0.1353	0.13344, 0.13417, 0.13455
κ_{crit}	0.13581^{+2}_{-1}	0.13525^{+2}_{-1}
κ_{n}	0.13578^{+2}_{-1}	0.13520^{+1}_{-2}
κ_{s}	0.13495^{+2}_{-2}	0.13401^{+2}_{-2}

Table 1: Input and derived parameters. The lattice spacing is set by r_0 .

parameter which corresponds to zero quark mass, κ_{s} and κ_{n} are taken from [13] where the lattice spacing has been fixed from the Sommer scale r_0 [14, 15]. Statistical errors are estimated using the bootstrap [16] with 1000 re-samplings. Unless otherwise specified, all errors listed in tables are statistical.

Non-perturbative determinations of the improvement coefficients are available from two groups. The ALPHA collaboration have determined the value of c_{SW} [17, 18] using chiral symmetry and Ward identities in the Schrödinger Functional (SF) formalism. They have determined c_A [18] and Z_A , Z_V and b_V [19] in the same scheme and have a preliminary determination of c_V [20, 21]. Bhattacharya *et al.* [22, 23, 24] have determined all the improvement coefficients needed to improve and renormalise quark bilinears, also using Ward identities, but on a periodic lattice with standard sources. They also use the ALPHA value of c_{SW} to improve the action. The values of Z_V , Z_A and b_V are in good agreement between the two groups. However, the ALPHA values for c_V and c_A are much larger than those of Bhattacharya *et al.* In a more detailed discussion of the improvement coefficients [25] we noted that the matrix elements determining leptonic decays are particularly sensitive to the value of the mixing c coefficients. As shown in equation (2.2) it is the derivative of a current which is the improvement term. For the decay constants calculated at zero

three-momentum the derivative is the mass of the state which is $\mathcal{O}(1)$. For the matrix elements determined here, the momentum component is a momentum difference and is $\mathcal{O}(1/10)$. Thus these matrix elements are relatively insensitive to the values of the mixing coefficients. We use the value of Bhattacharya *et al.* The value of b_m is determined in lattice perturbation theory [26] with the boosted coupling $g^2 = g_0^2/u_0^4$ [27]. The mean link, u_0 , is taken from the plaquette expectation value, $u_0^4 = \langle \text{Re Tr } U_P \rangle / 3$. The values of the improvement coefficients are shown in table 2.

2.3 Correlation functions

Details of the fitting procedure, and extraction of the spectrum and amplitudes between the vacuum and meson states at zero three-momentum: $\langle M_P | \bar{\psi} \gamma_5 \psi | 0 \rangle$ for example can be found in [13, 25]. We used the fuzzing smearing function [28] for the light quark propagators and a hydrogenic gauge invariant function [29] for the heavy quarks.

The light-light 2-point correlation functions at non-zero momentum were somewhat noisy. To determine these as accurately as possible we used a constrained dispersion relation fit. That is, we constrained the energy of the non-zero momentum states to be

$$E^2(|\vec{p}|^2) = M^2 + \vec{p} \cdot \vec{p} \quad (2.7)$$

Furthermore, we constrained the amplitudes by fitting the correlator which was fuzzed at source and local at sink (FL) to the following form

$$C(\vec{p}, t) = \frac{Z^F(|\vec{p}|^2) Z^L}{2E} \left(e^{-Et} + e^{-E(T-t)} \right) \quad (2.8)$$

where T is the time extent of the lattice and E is constrained from equation (2.7). The local Z^L , by Lorentz invariance, is not a function of momentum and so both Z^L and M are determined at zero momentum.

We determined the amplitudes and energies of the heavy-light mesons at all momenta using a free single exponential fit. We then compared to the dispersion relation as a check of lattice artefacts.

We have extracted the matrix element for the semileptonic decays from three-point and two-point correlation functions. The three-point function for the transition from state A to state B is given by,

$$C_{3\text{pt}}^\mu(\vec{p}, t_x, \vec{k}, t_y) = \sum_{\vec{x}, \vec{y}} e^{-i(\vec{k} \cdot \vec{x} + (\vec{k} - \vec{p}) \cdot \vec{y})} \langle 0 | \mathcal{T} \{ \Omega_B(x) J^\mu(y) \Omega_A^\dagger(0) \} | 0 \rangle \quad (2.9)$$

where Ω_A^\dagger is the operator which creates state A , Ω_B is the operator which destroys state B and J^μ is the weak current. We have computed the correlation function using the “standard

	$\beta = 6.2$	$\beta = 6.0$
c_{SW}	1.614	1.769
Z_A	0.818(2)(5)	0.807(2)(8)
b_A	1.32(3)(4)	1.28(3)(4)
c_A	-0.032(3)(6)	-0.037(4)(8)
Z_V	0.7874(4)	0.770(1)
b_V	1.42(1)(1)	1.52(1)
c_V	-0.09(2)(1)	-0.107(17)(4)
b_m	-0.6517	-0.6621

Table 2: Improvement coefficients used in this work.

source” method [30, 31]. We chose the extension timeslice to be, $t_x = 28$ rather than in the centre of the lattice at $t = 24$. This enabled us to look for different systematic effects by comparing both sides of the lattice, for example to look at different time orderings of operators and to check the quality of plateaux. However, we lost the ability to average results from the front and back sides of the lattice and so our statistical errors are larger.

When the operators are well separated, that is when t_y and $t_x - t_y$ are large, then

$$C_{3\text{pt}}^\mu(\vec{p}, t_x, \vec{k}, t_y) = \frac{e^{-E_B t_y}}{2E_B} Z_A \frac{e^{-E_\rho(t_x - t_y)}}{2E_\rho} Z_B^* \langle \rho(\vec{k}) | J^\mu(0) | \bar{B}(\vec{p}) \rangle \quad (2.10)$$

where $Z_i = \langle 0 | P_i | P_i(\vec{p}_i) \rangle$. Both the Z ’s (for smeared operators) and the energies are functions of three-momentum squared, $|\vec{p}_i|^2$, and can be extracted from the appropriate two-point functions, as described above. The remaining matrix element is the one in equation (1.1).

The simulation used heavy meson spatial momentum of magnitude 0 or 1, in lattice units of $2\pi/aL$. The light meson was given spatial momentum of 0 or 1 in lattice units. Six momentum channels with different values of q^2 were considered, shown in table 3.

channel	\vec{p}	\vec{k}		$\langle \rho A_\mu B \rangle$	$\langle \rho V_\mu B \rangle$
0	(0, 0, 0)	(0, 0, 0)		1	0
1	(0, 0, 0)	(1, 0, 0)	+perms	5	1
2	(1, 0, 0)	(1, 0, 0)		3	2
3	(1, 0, 0)	(0, 0, 0)	+perms	4	2
4	(1, 0, 0)	(0, 1, 0)	+perms	10	3
5	(1, 0, 0)	(-1, 0, 0)		5	1

Table 3: Values of three-momentum in lattice units of $\frac{2\pi}{aL}$ and the number of distinct matrix elements for each momentum channel. “+ perms” implies permutations of \vec{k} that have the same q^2 ,

For each channel, different spatial and temporal components combined with the relevant three-momentum allow equations (1.1) to be decomposed into distinct matrix elements. The three-point correlation functions were fitted simultaneously to the distinct matrix elements with the form factors as free parameters. We averaged over momenta and Lorentz channels that have the same matrix element. The number of distinct matrix elements for each channel and current is shown in Table 3. For channel 0, the coefficients vanish for all the form factors except A_1 .

Figure 1 shows examples of the averaged three-point correlation functions with the time dependence divided out. The data on the fore-side of the lattice has larger statistical errors. This is simply due the noise-to-signal ratio increasing at larger time separations. We observed clear plateaux, but note that the plateaux on the back-side of the lattice are better for extracting the signal. We chose to fit to the three-point function with the time-dependence cancelled using fitted two point functions rather than use the ratio of three-point over two-point correlation functions as the current operator has less overlap

with excited states. This is supported by the data, as we see longer plateaux when using the fitted two-point parameters.

It is clear that even on the shorter back-side of the lattice the separation of the operators is sufficient to see only the ground state. For the spatial current (open symbols) there is a significant disagreement between each side of the lattice. This may be due to contamination from different time orderings of the operators wrapping around the lattice. In this case, one would expect the shorter back-side of the lattice to be less affected than the longer fore-side.

In general, we fitted to the central five timeslices on the back side of the lattice. For several channels we have shifted this window to accommodate a better plateau. Some channels had much clearer plateaux on the fore-side of the lattice. In all cases the criteria for choosing the fit range was a plateau such that the form factors were stable against a change of one timeslice in the fit range and that had a reasonable reduced χ^2 and Q -value. We used a block diagonal covariance matrix to prevent different systematics between different currents being misinterpreted as correlation information.

By measuring the quark mass dependence of the form factors, we can interpolate and/or extrapolate to the quark masses of the physical decays we are interested in.

2.4 Light quark dependence

In quenched lattice QCD calculations, light quarks are typically simulated around the strange quark mass and then extrapolated to light or zero quark mass. The reasons for this are mainly algorithmic and computational. In the first instance, the computation of light quark propagators suffers from critical slowing down. The number of iterations it takes to invert the fermion matrix varies inversely with the quark mass, making light quarks prohibitively expensive in computer time. Second, as the quarks become lighter the hadron states become larger, requiring a larger box size, again increasing the amount of computation required. Third, quenched QCD has the wrong chiral behaviour, but in practice it is the computational requirements which restrict the range of quark mass.

The form factor F has both explicit, and implicit mass dependence,

$$F = F(q^2(m_A, m_P), m_A, m_P) \quad (2.11)$$

where m_A is the active quark mass and m_P is the passive quark mass. For small changes in m_A , m_P , and q^2 the variation in the form factor can be approximated by a first-order

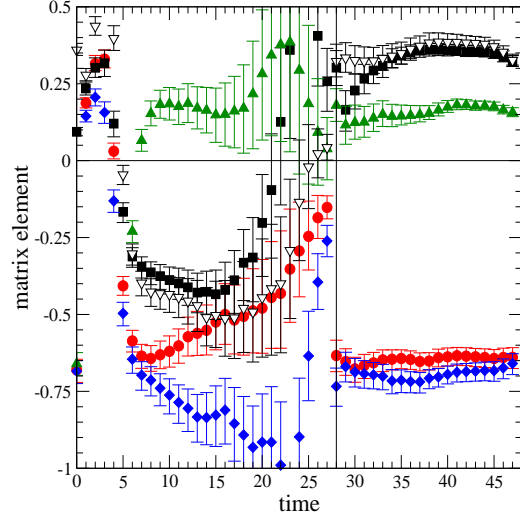


Figure 1: C_{3pt} with measured two-point factors divided off, for $\beta = 6.2$, light quarks, $\kappa_A = \kappa_P = 0.1346$ and the heavy quark, $\kappa = 0.1200$, kinematic channel 1. Different symbols show the distinct matrix elements for $\langle V|A|P \rangle$.

Taylor expansion

$$F(q^2, m_A, m_P) = \alpha + m_A \frac{\partial F}{\partial m_A} + m_P \frac{\partial F}{\partial m_P} + q^2 \frac{\partial F}{\partial q^2} \quad (2.12)$$

For a particular momentum channel the exact dependence of q^2 on meson mass is known. The first-order Taylor expansion of q^2 gives

$$q^2 = \beta + \gamma M_H + \delta M_L \quad (2.13)$$

where M_H is the mass of the heavy pseudoscalar meson and M_L is the mass of the light state. To a good approximation M_H varies linearly with m_P . The light vector meson mass depends linearly on the averaged light quark mass $m_{\text{eff}} = (m_A + m_P)/2$.

To control this extrapolation, we separated the chiral and momentum behaviour of the form factors by first interpolating in q^2 , at fixed quark mass, to a common set of q^2 values over the range of quark masses. Then we extrapolated in quark mass at fixed q^2 , as suggested by [32]. To interpolate the form factors in q^2 , we used pole models [33, 34, 35],

$$F(q^2) = \frac{F(0)}{1 - q^2/m_F^2} \quad (2.14)$$

This is illustrated in figure 2. As we have interpolated in q^2 any model dependence will be small. We have checked for residual model dependence by varying the model. The figure shows the form factors and the pole mass fits. We note that before any heavy quark extrapolation we can cover the full range of physical q^2 values.

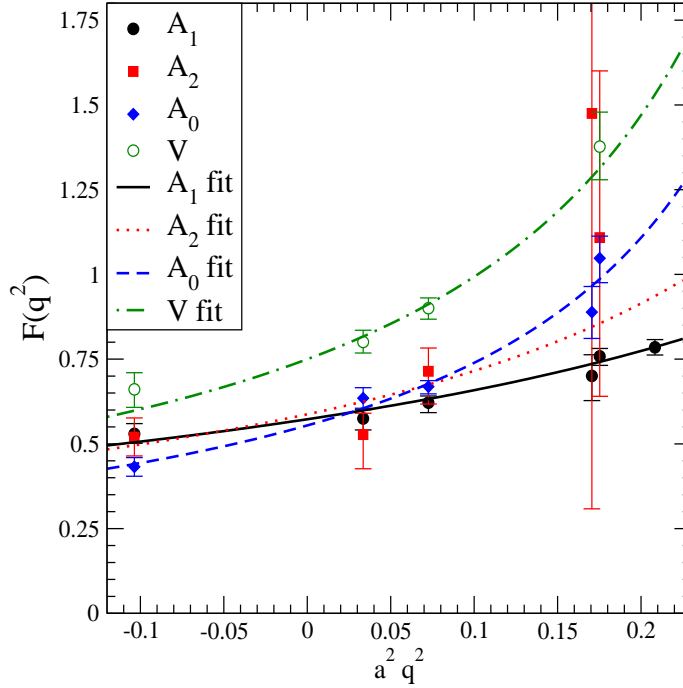


Figure 2: The form factors as a function of q^2 , at $\beta = 6.2$ for $\kappa_H = 0.1200$, $\kappa_A = \kappa_P = 0.1346$.

Once the q^2 dependence of the form factors had been determined, we chose a set of common q^2 values to which we interpolated at each value of the quark mass. We then extrapolated the form factors at fixed q^2 in two dimensions according to

$$F(m_{\text{eff}}, m_P) \Big|_{q^2=\text{const}} = \alpha + \beta m_P + \gamma m_{\text{eff}} \quad (2.15)$$

2.5 Heavy quark extrapolation

Near zero-recoil (q_{max}^2) the form factors scale in the following way [36],

$$F \sim M^{N/2} \quad (2.16)$$

where $N = 1$ for $F \in \{V, A_0, A_2\}$, $N = -1$ for $F = A_1$. We introduce a new kinematic variable

$$v \cdot k = \frac{M_H^2 + M_L^2 - q^2}{2M_H} \quad (2.17)$$

where v is the four-velocity of the heavy meson. We then have the following form for the extrapolation at fixed $v \cdot k$.

$$\Phi_i \equiv C(M_H, M_B) F(v \cdot k) M^{-N/2} = \zeta \left(1 + \frac{\eta}{M_H} + \frac{\theta}{M_H^2} + \dots \right) \quad (2.18)$$

The coefficient C is the logarithmic matching factor [37],

$$C(M_H, M_B) = \left(\frac{\alpha_s(M_B)}{\alpha_s(M_H)} \right)^{2/\beta_0} \quad (2.19)$$

where $\beta_0 = 11$ in quenched QCD and α_s is the one-loop running coupling with $\Lambda_{\overline{MS}}^{(4)} = 295 \text{ MeV}$.

With the fixed- q^2 extrapolation, it is easy to implement the heavy quark extrapolation. We used a different set of q^2 at each value of the heavy quark mass so that the heavy quark extrapolation could be done at fixed $v \cdot k$.

Figure 3 shows the extrapolation of the form factor A_1 . The solid line shows the quadratic fit to all four data points at $\beta = 6.2$, and the dot-dashed line shows the linear fit to the heaviest three. At the B meson mass the two lines are still close together, suggesting that the extrapolation is reasonable. Comparing the circles ($\beta = 6.2$) with the squares ($\beta = 6.0$) there is little difference, suggesting that $\mathcal{O}((am)^2)$ lattice artefacts are small. In [25] we fitted simultaneously to the data for the decay constants at both lattice spacings, allowing for lattice artefacts, and found the effect to be small. The method of extrapolation is the same as used here. However, we do not attempt a simultaneous fit since the statistical precision of the data is not sufficiently good even for A_1 .

3. Results

In principle one could compute the form factors for any value of q^2 from lattice QCD. However, states with high spatial momentum are very noisy and thus difficult to measure

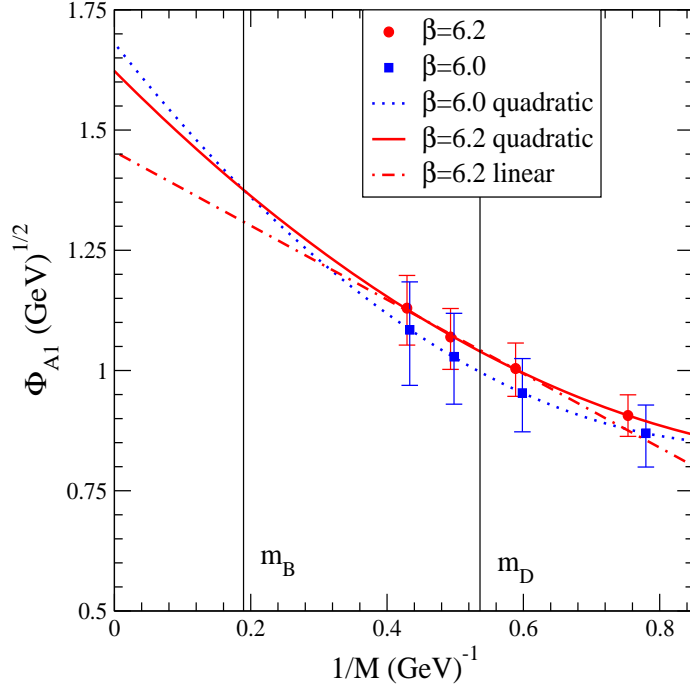


Figure 3: The heavy quark extrapolation for the form factor A_1 at the highest value of q^2 .

on the lattice. Thus we are restricted to the high q^2 end of the range. In addition, the procedures we have introduced to control the extrapolations, separating the q^2 from the quark mass dependence, have further restricted the range of q^2 away from q_{max}^2 , in the range

$$12.7 \text{ GeV}^2 \leq q^2 \leq 18.2 \text{ GeV}^2 \quad (3.1)$$

Moreover, the relatively small number of momentum channels for which the form factors are extracted, six for A_1 , five for A_0 and A_2 , and four for V , coupled with the interpolation at fixed q^2 imply by naive counting of degrees of freedom that we have only four independent data for A_1 and worse, two independent data for V . Fitting the functional form of the q^2 dependence of the form factors is thus rather hard. However, we are free to evaluate the form factors, and thus the differential decay rate, at any value of q^2 we choose without introducing any extra model dependence as long as it is in the range of allowed q^2 . In particular we can determine a partially integrated decay rate over this range.

Figure 4 shows the four form factors on both lattices. In this case we have chosen nine values of q^2 . The form factor A_1 which dominates at q_{max}^2 is well determined and is in good agreement for both lattice spacings. The subleading form factors have a much noisier signal, especially for the coarser lattice. This made the extrapolations very difficult to control. For the coarse lattice only we introduced two additional model dependent constraints on the data during the fixed quark mass q^2 interpolation. First, according to pole models the pole mass for A_1 and A_2 should be the same, and we enforce this constraint. As A_1 is much better determined than A_2 , A_1 remains unchanged. Second, we find a dipole rather than a pole fits the data better for V . Both these constraints affect the value of the form

factors very little for the fine lattice and are not required to control the extrapolations. As the finer lattice forms our result and the coarse lattice is used to estimate lattice artifacts, the resulting model dependence enters only in our estimate of systematic error.

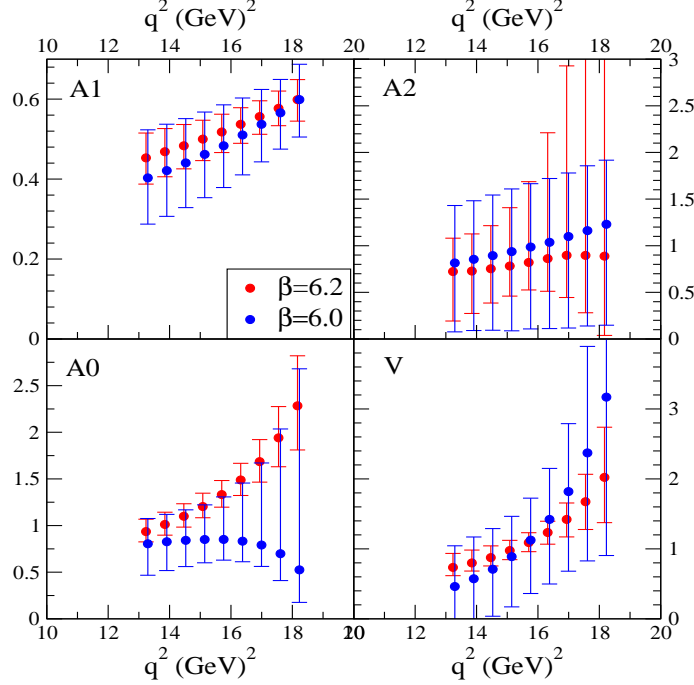


Figure 4: The form factors on both lattices. The vertical scale is different for each form factor.

In Table 4 we list the values of the form factors on both lattices at the highest and lowest values of q^2 only. Using equation (1.5) we can similarly determine the differential decay rate over the same range of momentum. Shown in figure 5 is the differential decay rate on both lattices. To reiterate, we can evaluate the differential decay rate for *any* q^2 in the allowed range but only two data points will be independent. For this reason, our main result is for the partially integrated decay rate over the allowed range given in equation (3.1)

$$\Gamma_{\text{PI}} = \int_{12.7 \text{ GeV}^2}^{18.2 \text{ GeV}^2} dq^2 \frac{\partial \Gamma}{\partial q^2} = 4.9^{+12+0}_{-10-14} \times 10^{12} \text{ s}^{-1} |V_{\text{ub}}|^2, \quad (3.2)$$

where the first error is statistical and the second is systematic. Estimates of systematic error are discussed in the next section.

The CLEO collaboration [38] have measured the rates for the decays $B \rightarrow \pi l \nu$ and $B \rightarrow \rho l \nu$. They determine the partial decay rate for three ranges of q^2 : $0 < q^2 < 8 \text{ GeV}^2$, $8 < q^2 < 16 \text{ GeV}^2$, and $q^2 \geq 16 \text{ GeV}^2$. They compare the measured partially integrated decay rate with Light Cone Sum Rules (LCSR) results for $q^2 < 16 \text{ GeV}^2$, and to lattice QCD data for $q^2 > 16 \text{ GeV}^2$. We cannot bin our data in the same way as we have not determined the form factors at q_{max}^2 , so we cannot directly compare. The BaBar collaboration [39] have measured the total decay rate, but only quote for the lifetime and V_{ub} , so again we cannot compare our results to the experimental data at the same values of q^2 .

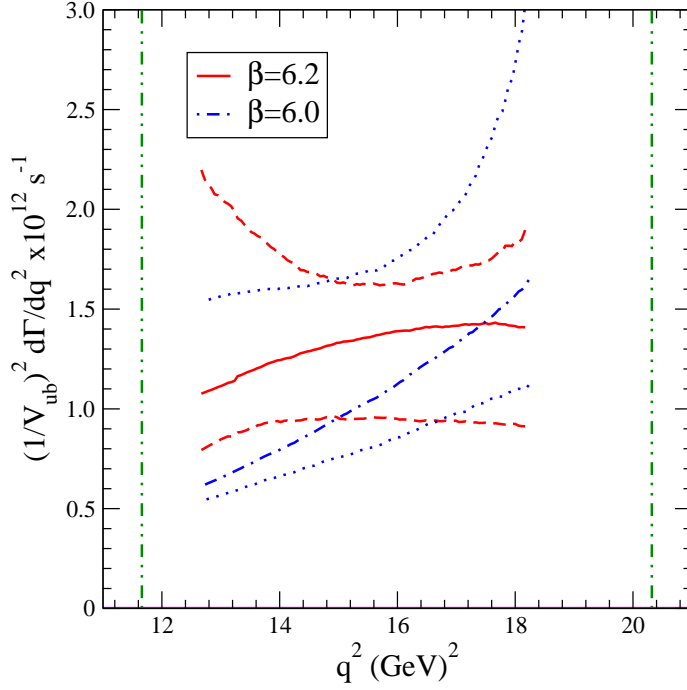


Figure 5: The differential decay rate on both lattices. The vertical line to the left is the charm end point, and to the right is q_{max}^2 .

3.1 Systematic uncertainties

This calculation is done in the quenched approximation. There is therefore an uncontrolled systematic error. For most dimensionful quantities such as the hadron spectrum this is of the order of 10%. The quenching error is manifest in the choice of quantity used to set the scale: in the quenched approximation different quantities such as the nucleon mass, or the Sommer scale, give different answers for the lattice spacing. The form factors are dimensionless and so are not directly affected by the scale-setting. However there is an indirect dependence. We vary the choice of quantity used to set the scale. This in itself is not an estimate of the quenching systematic on the form factors, only of their implicit scale dependence. We use the Sommer scale, r_0 to set the scale. At each lattice spacing the value of a/r_0 is unambiguously defined although the experimental value is not known. Sommer originally advocated $r_0 = 0.5 \text{ fm}$ but determinations of the lattice spac-

$q^2 \text{ (GeV)}^2$	$\beta = 6.2$	$\beta = 6.0$
A_1		
18.2	0.60^{+5}_{-5}	0.60^{+9}_{-9}
12.7	0.45^{+6}_{-7}	0.40^{+12}_{-12}
A_2		
18.2	0.88^{+500}_{-85}	1.23^{+69}_{-108}
12.7	0.72^{+36}_{-53}	0.82^{+62}_{-74}
A_0		
18.2	2.28^{+53}_{-47}	0.52^{+216}_{-35}
12.7	0.93^{+13}_{-11}	0.80^{+27}_{-34}
V		
18.2	2.02^{+72}_{-65}	3.17^{+247}_{-226}
12.7	0.74^{+20}_{-12}	0.46^{+58}_{-58}
$\frac{\partial \Gamma}{\partial q^2} \times 10^{12} \text{ s}^{-1}$		
18.2	1.4^{+5}_{-5}	1.6^{+16}_{-5}
12.7	1.1^{+10}_{-4}	0.6^{+9}_{-1}

Table 4: The form factors on both lattices

ing using the kaon decay constant, the nucleon mass or the rho mass correspond to r_0 values in the range 0.5–0.55 fm. We take $r_0 = 0.5$ fm as our central value and use $r_0 = 0.55$ fm to estimate the systematic error from quenching scale ambiguity.

We simulate heavy quarks with several quark masses around the charm quark mass and then use continuum heavy quark symmetry to extrapolate the form factors to the bottom quark mass. We estimate the systematic uncertainty coming from the quadratic extrapolation in equation (2.18) by performing a linear extrapolation to the heaviest three quark masses. This is shown as the dot-dashed line in figure 3. For the form factor A_1 on the finer lattice spacing at high q^2 this effect is smaller than the statistical uncertainty. For the other form factors the effect is larger, so we include this in the systematic uncertainty of the partially integrated decay rate.

In [25] we made several estimates of systematic uncertainty arising from the heavy-quark formalism and renormalisation method. We argue here that the same effects will be no larger for the form factors than for the heavy-light decay constants. We simultaneously fitted the heavy-light decay constant data at both lattice spacings and allowed for mass dependent lattice artefacts. This produced a 5% effect in the value of decay constant. We do not attempt this procedure here as our statistical errors are too large, but have no reason to believe it would be a greater effect for the form factors. As suggested by Bernard [40] the normalisation of the currents can be altered so that while formally the same at $\mathcal{O}(a)$ it looks much more like the mass dependent normalisation of the Fermilab formalism [7].

$$\psi \rightarrow \psi' = \sqrt{1 + \mu am} \psi \quad (3.3)$$

where μ depends on the improvement coefficients Z_J , c_J and b_J and the improved currents defined in equation (2.2). Combining this alternative normalisation with the kinetic mass M_2 defined as

$$\frac{1}{M_2} = \left. \frac{\partial^2 E}{\partial p_k^2} \right|_{\vec{p}=0} \quad (3.4)$$

we found that this produced an effect on the pseudoscalar decay constant smaller than the difference between the linear and quadratic extrapolations at the coarser lattice spacing. As we described in section 2.1, the effect of the improvement for the form factors is much smaller than for the decay constants, so the overall effect of changing the normalisation and hadron mass cannot be greater than for the decay constants. Finally we varied the values of the improvement coefficients by the errors quoted by Bhattacharya *et al.* [22] and found the overall effect to be 1% in the axial and 3% in the vector currents. Again, as the effect of improvement is smaller in the form factors the overall effect cannot be greater than this.

The main systematic uncertainties are tabulated in table 5. To obtain the systematic error on the partially integrated decay rate we have combined the systematic errors in quadrature.

	Γ_{PI}	$\frac{\partial\Gamma}{\partial q^2} _{\text{low}}$	$\frac{\partial\Gamma}{\partial q^2} _{\text{high}}$
lattice spacing	−20%	−45%	+14%
quenched scale ambiguity	−20%	−27%	−14%
heavy quark extrapolation	−16%	−9%	−14%
pole model dependence	−4%	−5%	+0%

Table 5: Systematic uncertainties in the decay rate

Acknowledgments

We thank PPARC for support under grants PPA/G/O/2002/00468, PPA/G/O/2002/00465 and PPA/G/S/2002/00467. We acknowledge EPSRC for support under grant GR/K41663

References

- [1] L. Wolfenstein, Phys. Rev. Lett. **51**, 1945 (1983).
- [2] Belle Collaboration, K. Abe *et al.*, hep-ex/0308036.
- [3] BABAR Collaboration, B. Aubert *et al.*, Phys. Rev. Lett. **89**, 201802 (2002).
- [4] J.G. Körner and G.A. Schuler, Phys. Lett. B **231**, 306 (1989).
- [5] F.J. Gilman and R.L. Singleton Jr., Phys. Rev. D **41**, 142 (1990).
- [6] B. Sheikholeslami and R. Wohlert, Nucl. Phys. B **259**, 572 (1985).
- [7] A.X. El-Khadra, A.S. Kronfeld, and P.B. Mackenzie, Phys. Rev. D **55**, 3933 (1997).
- [8] UKQCD Collaboration, K.C. Bowler *et al.*, Phys. Lett. B **486**, 111 (2000).
- [9] UKQCD Collaboration, J. Gill, Nucl. Phys. B (Proc. Suppl.) **106**, 391 (2002).
- [10] M. Creutz, Phys. Rev. D **36**, 2394 (1987).
- [11] F. Brown and T. Woch, Phys. Rev. Lett. **58**, 163 (1987).
- [12] N. Cabibbo and E. Marinari, Phys. Lett. B **119**, 387 (1982).
- [13] UKQCD Collaboration, K.C. Bowler *et al.*, Phys. Rev. D **62**, 054506 (2000).
- [14] R. Sommer, Nucl. Phys. **B411**, 839 (1994).
- [15] M. Guagnelli, R. Sommer and H. Wittig, Nucl. Phys. B **535**, 389 (1998).
- [16] B. Efron, SIAM Review **21**, 460 (1979).
- [17] M. Lüscher, S. Sint, R. Sommer and P. Weisz, Nucl. Phys. B **478**, 365 (1996).
- [18] M. Lüscher, S. Sint, R. Sommer, P. Weisz, H. Wittig and U. Wolff, Nucl. Phys. B (Proc. Suppl.) **53**, 905 (1997).
- [19] M. Lüscher, S. Sint, R. Sommer, and H. Wittig, Nucl. Phys. B **491**, 344 (1997).
- [20] R. Sommer, Nucl. Phys. Proc. Suppl **60A**, 279 (1998).
- [21] M. Guagnelli and R. Sommer, Nucl. Phys. B (Proc. Suppl.) **63A-C**, 886 (1998).
- [22] T. Bhattacharya *et al.*, Phys. Lett. B **461**, 79 (1999).

- [23] T. Bhattacharya, R. Gupta, W. Lee, S. Sharpe, Nucl. Phys. B (Proc. Suppl.) **83-84**, 851 (2000).
- [24] T. Bhattacharya, R. Gupta, W. Lee, S. Sharpe, Phys. Rev. D **62**, 074505 (2001).
- [25] UKQCD Collaboration, K.C. Bowler *et al.*, Nucl. Phys. B **619**, 507 (2001).
- [26] S. Sint and P. Weisz, Nucl. Phys. B **502**, 251 (1997).
- [27] G. Lepage and P. Mackenzie, Phys. Rev. D **48**, 2250 (1993).
- [28] P. Lacock, A. McKerrell, C. Michael, I.M. Stopher and P.W. Stephenson, Phys. Rev. D **51**, 6403 (1995).
- [29] P. Boyle, J. Comput. Phys. **179**, 349 (2002).
- [30] C. Bernard and A. Soni, Nucl. Phys. B (Proc. Suppl.) **9**, 155 (1989).
- [31] C. Bernard, in *Gauge Theory on a Lattice: 1984, Argonne National Laboratory Workshop*, edited by C. Zachos *et al.* (National Technical Information Service, Springfield, VA, 1984).
- [32] L. Lellouch, Nucl. Phys. B **479**, 353 (1996).
- [33] M. Bauer, B. Stech and M. Wirbel, Z. Phys. C **29**, 627 (1985).
- [34] M. Bauer, B. Stech and M. Wirbel, Z. Phys. C **34**, 103 (1987).
- [35] M. Bauer and M. Wirbel, Z. Phys. C **42**, 671 (1989).
- [36] N. Isgur and M. Wise, Phys. Rev. D **42**, 2388 (1990).
- [37] M. Neubert, Phys. Rev. D **49**, 1542 (1994).
- [38] CLEO Collaboration, S.B. Athar *et al.*, Phys. Rev. D **68**, 072003 (2003).
- [39] BaBar Collaboration, B. Aubert *et al.*, Phys. Rev. Lett. **90**, 181801 (2003).
- [40] C. Bernard, Nucl. Phys. B (Proc. Suppl.) **94**, 159 (2001).